analytical chemistry

Article

Cite This: Anal. Chem. 2018, 90, 2395−2400

pubs.acs.org/ac

Triple Signal Amplification Strategy for Ultrasensitive Determination of miRNA Based on Duplex Specific Nuclease and Bridge DNA−Gold Nanoparticles

Bing Bo,[†] Tian Zhang,[‡] Yiting Jiang,[‡] Haiyan Cui,*[,†] and Peng Miao*[,†,‡]

[†]Shanghai Pulmonary Hospital, Tongji University School of Medicine, Shanghai, 200433 P. R. China

[‡]Suzhou Institute of Biomedical Engineering and Technology, Chinese Academy of Sciences, Suzhou, 215163 P. R. China

Supporting Information

ABSTRACT: Abnormal expression of miRNAs always occurs in solid tumors. Thus, it is critical to sensitively and selectively detect such biomarkers for the diagnosis and prognosis of diseases. Here, we report a biosensing scheme for the determination of miRNA with triple signal amplification based on target-triggered cyclic duplex specific nuclease digestion and bridge DNA−gold nanoparticles. Electrochemical signals are recorded to present initial levels of miRNA. This method is ultrasensitive with a wide linear range of 10^{-17} to 10^{-11} M. The limit of detection is down to 6.8 aM. Moreover, the overexpression of miR-21 is confirmed in lung cancer patients by the proposed method, which is in good accordance with qRT-PCR results. In addition, the developed biosensor does not need a reverse transcription process or any thermal cycling processes. Its performance satisfies the requirement for convenient, rapid, sensitive, and specific early diagnosis of cancers. Therefore, it may have great potential utility in the near future.

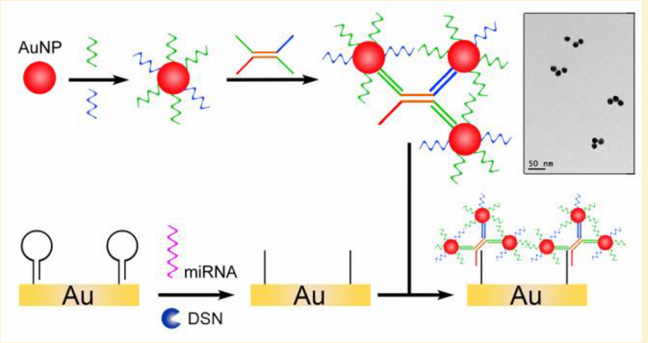

MicroRNAs (miRNAs) are a class of short noncoding RNAs (18−25 nucleotides) acting as sequence-specific post-transcriptional regulators.[1] They play critical roles in the cellular network of animals, plants, and protozoa.[2,3] miRNAs participate in various biological processes such as cell differentiation, proliferation, apoptosis, stress-specific cellular outcome, and tissue development.[4−7] Recently, many researches have focused on the convergent and cooperative miRNA network that drives angiogenesis and tumor metastasis.[8] It is also indicated that a number of diseases show abnormal expression of miRNAs; thus, they may serve as reliable disease biomarkers.[9,10] For instance, miR-21 is found to be a potential broad-spectrum biomarker for the detection of many cancers such as lung cancer,[11] hepatocellular carcinoma,[12] breast cancer,[13] lymphoma,[14] and glioma.[15]

Cancers are currently the most serious threats to human health, and the mortality is very high.[16] To understand the functions of miRNA in cancer diagnosis and chemotherapy response, accurate and sensitive detection of miRNA in biological samples is critical. Traditional techniques for miRNA analysis include Northern blotting analysis,[17] quantitative PCR,[18] and microarray.[19] However, due to the intrinsic features of miRNA such as short length, low expression level, and analogical sequences, improved methods are highly required to meet the latest analytical demands. So far, increasing interest in signal amplification has led to the development of many advanced nanomaterials such as luminescent quantum dots,[20] two-dimensional nanosheets,[21] and three-dimensional heterostructured nanocomposites.[22] Nucleic acid structure engineering is also an emerging hotspot, including hybridization chain reaction (HCR),[23] catalyzed-hairpin-assembly (CHA) amplification,[24] rolling circle amplification (RCA),[25,26] and strand displacement amplification (SDA).[27]

In this contribution, we introduce a novel amplified detection method for miRNA assay based on duplex specific nuclease (DSN) and bridge DNA−gold nanoparticles (AuNPs). This approach has several attractive features. First, DNA sequences are ingeniously designed to accurately control the aggregation of three AuNPs. The commonly undesired aggregation event is integrated in the triple signal amplification process, which also involves DSN-assisted cleavage cycles and AuNPs based enrichment of electrochemical species. Thus, ultrahigh sensitivity is promised for the detection of miRNA. Second, "turn-off" mode of biosensors always has low signal/background ratio, and certain nonspecific disturbances may lead to false positive results. Because the capture of signals is activated in the presence of target miRNA, this method belongs to the "turn-on" biosensor, which has intrinsic merits over traditional

Received: December 28, 2017
Accepted: January 8, 2018
Published: January 8, 2018

DOI: 10.1021/acs.analchem.7b05447
Anal. Chem. 2018, 90, 2395−2400

turn-off biosensors.[28] Third, it does not require any reverse transcription process, and thermal cycling is eliminated, which benefits practical applications and challenges the technique of qRT-PCR. Fourth, this strategy is highly generalized, which is applicable to different DNA and RNA sensing tasks. Therefore, further biomolecular sensing applications may be extended.

EXPERIMENTAL SECTION

Materials and Reagents. Gold(III) chloride trihydrate ($HAuCl_4 \cdot 3H_2O$), tris(2-carboxyethyl)phosphine hydrochloride (TCEP), trisodium citrate, diethypyrocarbonate (DEPC), ethylenediaminetetraacetic acid (EDTA), mercaptohexanol (MCH), and hexaammineruthenium(III) chloride ($[Ru(NH_3)_6]^{3+}$) were purchased from Sigma (United States). All other reagents were of analytical grade and were used as received. Water used in this work was purified by a Millipore system (18 MΩ·cm resistivity). It was further treated with DEPC (0.1%) before use. DSN was supplied by Genomax Technologies Pte Ltd. (Singapore). qRT-PCR kit was purchased from Life Technologies (United States). All oligonucleotides were synthesized and purified by Takara Biotechnology Co., Ltd. (Dalian, China). Detailed sequences are shown in Table S1.

Instrumentation. Transmission electron micrograph (TEM) was taken using an FEI Tecnai G20 transmission electron microscope (FEI Company, United States). Dynamic light scattering (DLS) characterization was performed using a Zetasizer Nano ZS90 (Malvern Instruments, UK). Electrochemical experiments were performed on a CHI 660D electrochemical workstation (CH Instruments, China). A traditional three electrode system was utilized, which consisted of a saturated calomel reference electrode, a platinum wire auxiliary electrode, and a gold working electrode. Electrochemical impedance spectroscopy (EIS) experiments were performed using 5 mM $[Fe(CN)_6]^{3-/4-}$ containing 1 M KCl with the parameters of 0.21 V bias potential, 5 mV amplitude, and 0.1−100 000 Hz frequency range. Chronocoulometry experiments were performed in 10 mM Tris-HCl solution containing 50 μM $[Ru(NH_3)_6]^{3+}$. The pulse period was 250 ms.

Gold Electrode Treatment. The substrate gold electrode with the diameter of 3 mm was first soaked in piranha solution (98% H_2SO_4:30% H_2O_2 = 3:1) for about 5 min (Caution: highly corrosive). It was rinsed with double-distilled water and then polished to a mirror-like surface using P5000 silicon carbide paper and 1, 0.3, and 0.05 μm alumina slurry, successively. After that, to remove any residual alumina, the electrode was sonicated in ethanol and then double-distilled water, respectively. The electrode was further incubated with 50% nitric acid for 0.5 h and then electrochemically cleaned with 0.5 M H_2SO_4. Afterward, it was dried by nitrogen and then incubated with 0.5 μM capture probe (10 mM Tris-HCl, 10 mM TCEP, 1 mM EDTA, 0.1 M NaCl, pH 7.4) for 10 h. Subsequently, the electrode was washed and then immersed in 0.1 M MCH for 0.5 h.

Preparation of Bridge DNA−AuNPs Nanocomposites. Bare AuNPs were synthesized according to a previous report.[29] Briefly, the solutions of $HAuCl_4$ (0.01%, w/v) and trisodium citrate (1%, w/v) were prepared separately. After 100 mL of $HAuCl_4$ was boiled, 3.5 mL of trisodium citrate was injected to the refluxing solution under violent stirring for 15 min. Next, the mixture solution was cooled slowly, but the stirring continued for another 30 min. Bare AuNPs were thus synthesized, which were purified by 3 cycles of centrifugation at 12 000 rpm for 30 min.

Two thiolated probes (DNA probes 1 and 2) was dissolved in Tris-HCl buffer solution (10 mM, 10 mM TCEP, 1 mM EDTA, 0.1 M NaCl, pH 7.4). Two μM DNA probe 1 and 1 μM DNA probe 2 we incubated in 1 mL of AuNPs. After 16 h, the DNA−AuNPs conjugates were aged in phosphate buffered saline (10 mM, pH 7.0) with 0.1 M NaCl for 24 h. The multifunctional AuNPs were purified by removing the excess reagents through centrifugation process. The precipitate was redispersed in 1 mL of phosphate buffered saline (10 mM, pH 7.4) with 0.2 M NaCl.

Bridge DNA were formed by the hybridization of two single-stranded DNA probes. Briefly, bridge DNA probe 1 and 2 were separately dissolved in phosphate buffered saline (10 mM, pH 7.4) with 0.2 M NaCl. The concentration of each DNA probe was 8 μM. The two solutions were mixed with equal volumes and heated to 95 °C for 2 min. After being cooled to room temperature, the formed bridge DNA was mixed with the multifunctional AuNPs for 2 h. Subsequently, the formed nanocomposites were purified by centrifugation and redispersion.

Capture Probe Activation and Nanocomposites Recruitment. Capture probe modified gold electrode was immersed in the 50 mM Tris-HCl (0.1 U DSN, 5 mM $MgCl_2$, 1 mM DTT, pH 8.0) which was previously spiked with different concentrations of miRNA. After reacting at 50 °C for 2 h, the electrode was carefully rinsed by 10 mM Tris-HCl containing 0.5% Tween and then pure water, respectively. The pretreated electrode was further immersed in the bridge DNA−AuNPs for 1 h before being transferred to the electrochemical system for measurement.

RESULTS AND DISCUSSION

Sensing Principle. The principle behind the amplified electrochemical detection of miRNA is illustrated in Scheme 1.

Scheme 1. Illustration of the Electrochemical Approach for Triple Amplified Detection of miRNA

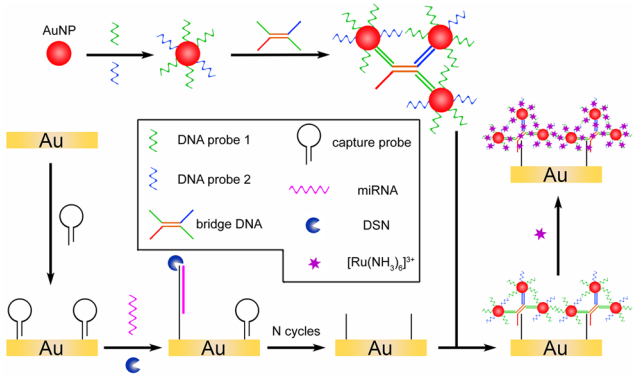

Generally, multifunctional AuNPs are constructed by mixing AuNPs with two thiolated DNA (DNA probes 1 and 2) via gold−sulfur chemistry. Next, by the hybridization of two partially complementary sequences (bridge DNA probes 1 and 2), bridge DNA is formed with a double-stranded middle section and four single-stranded tails. Two are designed to hybridize with DNA probe 1, and one is designed to hybridize with DNA probe 2. In addition, the last single-stranded tail is left for further electrode localization. Therefore, the bridge

DOI: 10.1021/acs.analchem.7b05447
Anal. Chem. 2018, 90, 2395−2400

DNA links three AuNPs specially to form the DNA nanocomposites. For the fabrication of the electrochemical miRNA biosensor, the gold working electrode is first cleaned, which is then immobilized with thiolated capture probe. The hairpin structure of the DNA probe is inactivated to capture bridge DNA−AuNPs. However, after the introduction of target miRNA, the hairpin is opened, and the formed DNA/RNA duplex can be recognized by DSN, which digests DNA in the duplex. The remained DNA sequence is activated, which hybridizes with the fourth single-stranded end of bridge DNA to localize the DNA nanocomposites. Meanwhile, miRNA is released, which triggers more cycles of capture probe activation and bridge DNA−AuNPs localization events. This strategy involves triple signal amplification. First, target miRNA triggers cycles of DSN-catalyzed digestion reaction for further localization of electrochemical signals; second, the bridge DNA−AuNPs contains three nanoparticles, and thus the density of AuNPs on the electrode surface is enhanced compared with the case of single DNA modified AuNPs. Third, because the AuNPs with large surface area are attached with numerous DNA probes, which absorb $[Ru(NH_3)_6]^{3+}$ via electrostatic interaction, significant electrochemical response can be obtained to indicate the initial level of miRNA.

Characterization of AuNPs and Electrode Interface. The synthesized AuNPs and constructed nanocomposites of bridge DNA−AuNPs were characterized by TEM. Figure 1a indicates that the prepared AuNPs are spherical with average size of 13 nm and are well-dispersed. The result is also consistent with DLS characterization (Figure S1). In the case of bridge DNA−AuNPs, three nanoparticles are combined by the bridge DNA. The phenomenon can be clearly observed in the TEM image (Figure 1b), demonstrating the successful construction of the nanocomposites. This commonly undesired aggregation event is used to enhance the final signals by accurate control of DNA sequences.

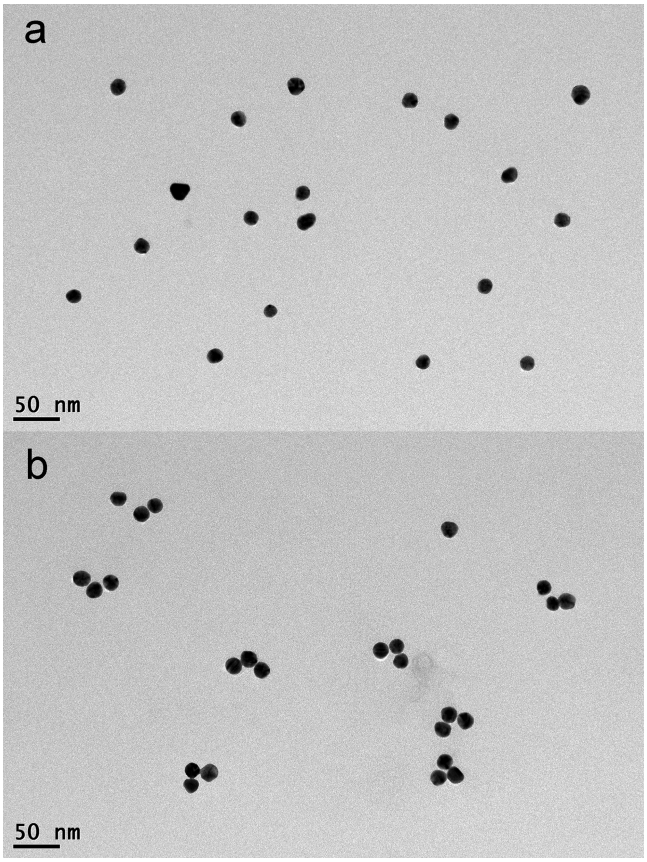

Figure 1. TEM images of (a) freshly prepared AuNPs and (b) bridge DNA−AuNPs.

The electrode interface modified with capture probe is then investigated by chronocoulometry. The coverage density of capture probe is estimated by the measurement of $[Ru(NH_3)_6]^{3+}$.[30] According to the Cottrell equation, the sum of the charge from the reaction of $[Ru(NH_3)_6]^{3+}$ and double layer charge equals the chronocoulometric intercept (charge versus $t^{1/2}$). By comparing the chronocoulometry curves of bare MCH modified electrode and capture probe modified electrode, the charge from the reaction of $[Ru(NH_3)_6]^{3+}$ can be obtained (Figure S2). The coverage density of capture probe is further calculated by referring to the equation:

$$\Gamma = \frac{Q}{nAF}$$

in which, Γ stands for the surface coverage density, A stands for the area of the electrode surface, n is the number of electrons transferred in one redox reaction, F is the Faraday constant, and Q is the obtained charge. Finally, the surface density of capture probe is calculated to be 1.79 pmol cm^{-2}.

Electrochemical Behavior of the Electrochemical Sensor. The molecular events occurred on the electrode surface can be studied by the techniques of EIS and chronocoulometry. As shown in Figure 2a, a straight line is observed in the Nyquist diagram, indicating the fine conductivity of the bare electrode (curve i). After modified with capture probe, a semicircle domain appears, which is due to the interfacial charge transfer resistance from the repellent between DNA phosphate backbone and $Fe(CN)_6^{3-/4-}$ (curve ii). In the absence of miRNA, DSN cannot digest capture probe, and thus the semicircle barely changes (curve iii). In addition, because the capture probe is not activated, bridge DNA−AuNPs cannot be effectively loaded, and the semicircle does not increase significantly (curve v). Only after the hybridization of miRNA and capture probe, DSN-assisted cleavage cycles can be conducted, and the semicircle decreases with shorter DNA on the electrode surface (curve iv). The activated capture probe hybridizes with bridge DNA−AuNPs and then localizes the nanocomposites on the electrode surface, which is reflected by the remarkably increased semicircle (curve vi). EIS result is in agreement with that of chronocoulometry. As shown in Figure 2b, the charge of electrochemical species is decreased only with the miRNA-triggered capture probe digestion. In addition, we studied the amplification efficiency of bridge DNA−AuNPs. Chronocoulometry curves of activated capture probe modified electrode before and after the loading of AuNPs are compared (Figure 3c). DNA probe 3 is designed with complementary sequence of activated capture probe. However, the localization of DNA probe 3 modified AuNPs contributes only to limited increase of charge. On the other hand, the bridge DNA combines three AuNPs, which leads to significant increase of charge value (Figure 3d). This result demonstrates that the design of bridge DNA−AuNPs is beneficial to signal enhancement compared with single AuNP-mediated signal amplification.

Quantitative Detection of Target miRNA. As shown in Figure 3a, we recorded the curves of capture probe modified electrode before and after DSN-assisted cleavage reaction in the

DOI: 10.1021/acs.analchem.7b05447
Anal. Chem. 2018, 90, 2395−2400

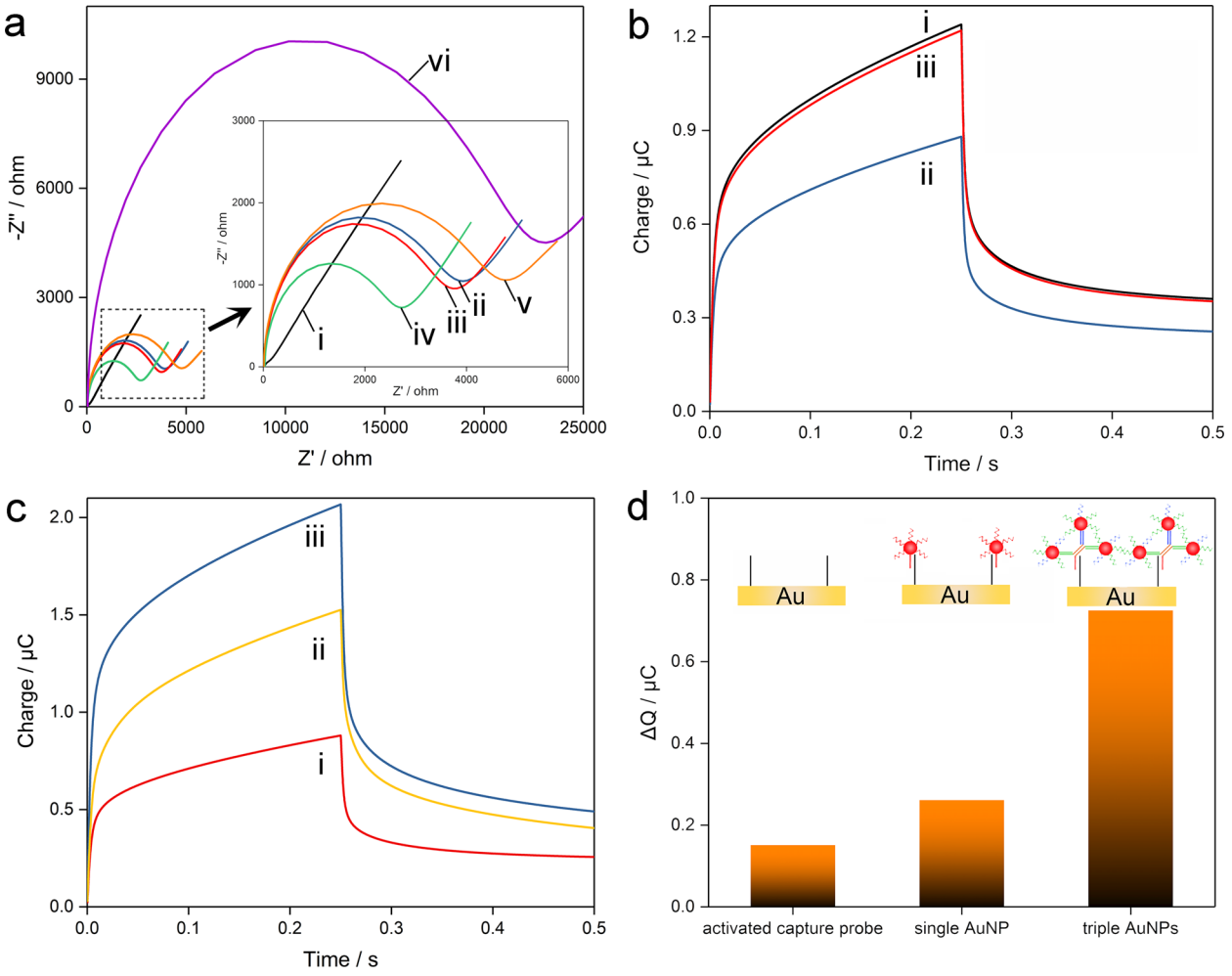

Figure 2. (a) Nyquist diagrams corresponding to (i) bare electrode, (ii) capture probe modified electrode, after DSN-assisted digestion in the (iii) absence and (iv) presence of miRNA, and further loading of bridge DNA–AuNPs after DSN-assisted digestion in the (v) absence and (vi) presence of miRNA. (b) Chronocoulometry curves for (i) capture probe modified electrode and after DSN-assisted cleavage reaction in the (ii) presence and (iii) absence of miRNA. (c) Chronocoulometry curves for (i) capture probe modified electrode after DSN-assisted cleavage reaction in the presence of miRNA, (ii) after capture of DNA probe 3 modified AuNPs, (iii) after capture of bridge DNA–AuNPs. (d) Corresponding variation of charge values.

presence of different amount of miRNA. With the increase of the concentration of miRNA, more capture probes are cleaved, thus the chronocoulometry curves are becoming lower. The chronocoulometric intercept (charge versus $t^{1/2}$) is defined as Q2. In addition, the curves after further loading of bridge DNA–AuNPs are also recorded. Larger amount of miRNA creates more activated capture probe for the immobilization of AuNPs, thus higher chronocoulometry curves are achieved. The corresponding chronocoulometric intercept (charge versus $t^{1/2}$) is defined as Q1. The ratio of Q1 to Q2 may be an excellent index of the concentration of miRNA compared with single charge values. We then studied the relationship between Q1/Q2 and miRNA concentration. A linear range from 10^{-17} to 10^{-11} is obtained with the fitting equation of

$$y = 6.13 + 0.30x \ (n = 3,\ R^2 = 0.99)$$

in which y is the value of Q1/Q2 and x is the logarithmic miRNA concentration. The semilog relationship is ascribed to the triple amplification process. The limit of detection is calculated to be 6.8 aM, which is lower than most previously reported electrochemical protocols (Table 1).

Selectivity and Practical Utility Investigation. To evaluate the selectivity of this novel method, three single-mismatched miRNA sequences (see Table S1 for details) were chosen in the sensing system replacing target miRNA. Figure 4 shows the comparison of the chronocoulometry responses of target and mismatched miRNAs with the concentrations of 10 fM and 10 pM, respectively. The Q1/Q2 values of target miRNA are much higher than those of the other mismatched sequences, which confirms that the proposed method is able to discriminate target miRNA with high selectivity.

The expression of miR-21 is upregulated in numerous tissues and serum plasma, which is recognized as an oncomir. We tested the effectiveness of the developed biosensing system in the analysis of real biological samples by measuring miR-21 levels in serum samples from lung cancer patients and a healthy individual as a control. miR-21 concentrations of all patient cases are much higher than that of the healthy person, which are consistent with the results of a commercial qRT-PCR kit. Therefore, excellent practical utility of this method is demonstrated.

DOI: 10.1021/acs.analchem.7b05447
Anal. Chem. 2018, 90, 2395–2400

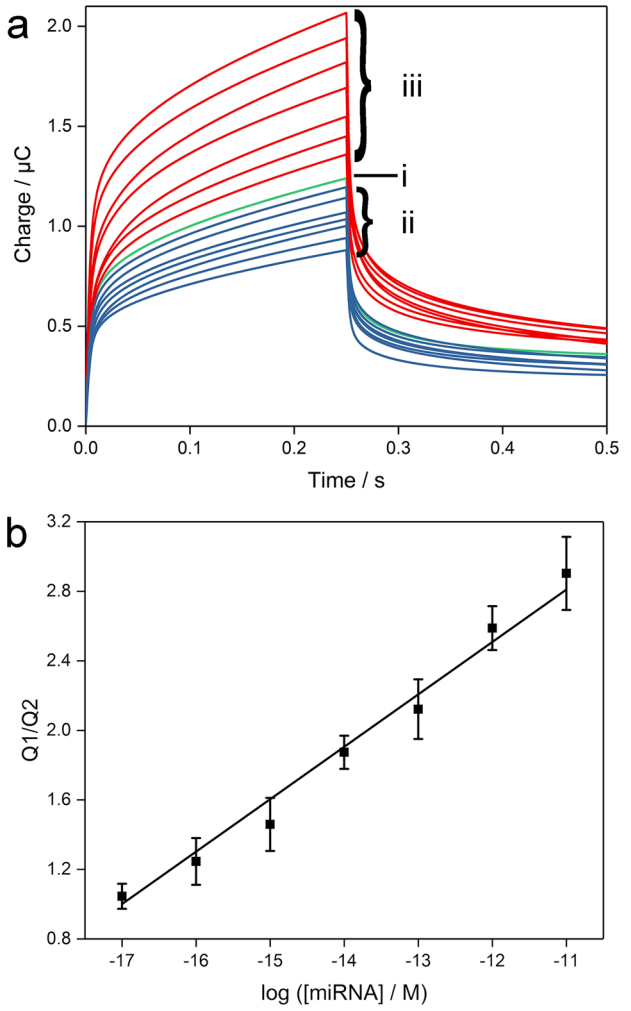

Figure 3. (a) Chronocoulometry curves for (i) capture probe modified electrode, (ii) after DSN-assisted cleavage reaction in the presence of miRNA (10^{-17} to 10^{-11} M, from top to bottom), and (iii) after further capture of bridge DNA–AuNPs (miRNA concentration: 10^{-17} to 10^{-11} M, from bottom to top). (b) The logarithmic calibration curve for miRNA concentration determination. The error bars represent relative standard deviations for three independent measurements.

CONCLUSIONS

In summary, we reported an electrochemical approach for the detection of miRNA based on DSN and bridge DNA–AuNPs. This miRNA assay is able to quantify miRNA down to 6.8 aM. The ultrahigh sensitivity originates from triple signal amplification combining DSN-assisted recycling of capture probe activation, AuNPs enrichment by bridge DNA, and numerous $[Ru(NH_3)_6]^{3+}$ concentrated around single AuNP. The method is also direct, without the need of reverse transcription process and any thermal cycling processes. In addition, it distinguishes target miRNA with low concentration from amounts of spurious analogues, which ensures excellent performance in real sample applications. This approach was successfully tested for the evaluation of miRNA in serum samples. We are confident that it may find practical applications of biomolecules assays and clinical diagnosis. We also believe this work will inspire future miRNA profiling methods and applications of DNA–AuNP nanocomposites.

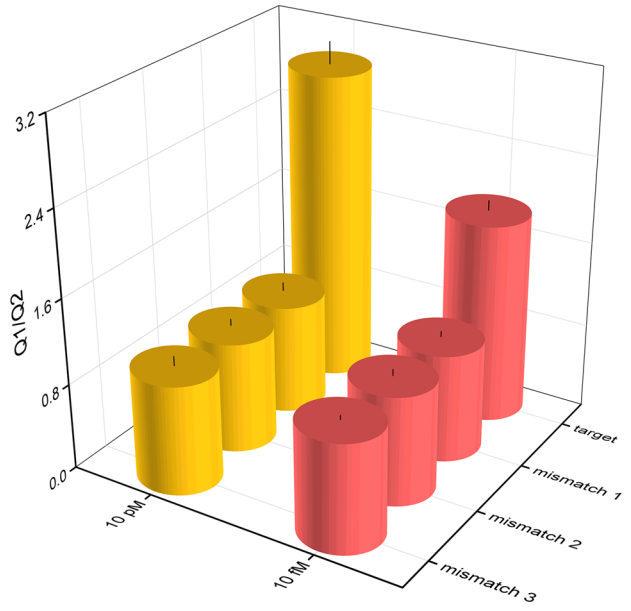

Figure 4. Selectivity assessment comparing Q1/Q2 values of target miRNA and mismatched miRNAs.

ASSOCIATED CONTENT

Supporting Information

The Supporting Information is available free of charge on the ACS Publications website at DOI: 10.1021/acs.analchem.7b05447.

DLS characterization of AuNPs, chronocoulometry curves for stepwise modified electrode, real sample analysis by the developed method, and DNA and RNA sequences used in the study (PDF)

Table 1. Comparison of the Analytical Performances of Recent Electrochemical miRNA Assays

technique	strategy	detection range (M)	LOD (M)	ref
differential pulse voltammetry	HCR with multiple G-quadruplex	10^{-12} to 8×10^{-10}	10^{-12}	31
square wave voltammetry	thionine and AuNPs cofunctionalized MoS_2 nanosheet	10^{-12} to 10^{-8}	2.6×10^{-13}	32
electrochemical impedance spectroscopy	AuNPs-decorated MoS_2 nanosheet	10^{-14} to 10^{-9}	4.5×10^{-16}	33
linear sweep voltammetry	tetrahedral DNA and SDA	10^{-15} to 10^{-9}	4×10^{-16}	34
square wave voltammetry	shape-controlled hierarchical Au nanostructures	10^{-16} to 10^{-13}	10^{-16}	35
square wave voltammetry	a triple-stem DNA redox probe	10^{-16} to 5×10^{-10}	10^{-16}	36
chronocoulometry	DSN and AuNPs	10^{-16} to 10^{-10}	5×10^{-17}	37
differential pulse voltammetry	Ru(III) release and redox recycling	10^{-16} to 1.5×10^{-12}	3.3×10^{-17}	38
amperometric *i*–*t* curve	HCR and catalytic enzymes	10^{-17} to 10^{-12}	10^{-17}	39
amperometric *i*–*t* curve	DNAzyme and DSN	5×10^{-17} to 5×10^{-16}	8×10^{-18}	40
chronocoulometry	DSN and AuNPs-bridge DNA nanocomposites	10^{-17} to 10^{-11}	6.8×10^{-18}	this work

DOI: 10.1021/acs.analchem.7b05447
Anal. Chem. 2018, 90, 2395–2400

AUTHOR INFORMATION

Corresponding Authors

*E-mail: miaopeng@sibet.ac.cn; Tel.: +86-512-69588279 (P.M.).

*E-mail: cuihaiyan@tongji.edu.cn (H.C.).

ORCID

Peng Miao: 0000-0003-3993-4778

Notes

The authors declare no competing financial interest.

ACKNOWLEDGMENTS

This work is supported by the National Natural Science Foundation of China (Grant 81771929), Science and Technology Program of Suzhou (Grant SYG201605), and China Postdoctoral Science Foundation (Grant 2017M611911).

REFERENCES

(1) Fabian, M. R.; Sonenberg, N.; Filipowicz, W. *Annu. Rev. Biochem.* **2010**, *79*, 351−379.

(2) Aguda, B. D.; Kim, Y.; Piper-Hunter, M. G.; Friedman, A.; Marsh, C. B. *Proc. Natl. Acad. Sci. U. S. A.* **2008**, *105*, 19678−19683.

(3) Zhang, Y. C.; Yu, Y.; Wang, C. Y.; Li, Z. Y.; Liu, Q.; Xu, J.; Liao, J. Y.; Wang, X. J.; Qu, L. H.; Chen, F.; Xin, P. Y.; Yan, C. Y.; Chu, J. F.; Li, H. Q.; Chen, Y. Q. *Nat. Biotechnol.* **2013**, *31*, 848−852.

(4) Fededa, J. P.; Esk, C.; Mierzwa, B.; Stanyte, R.; Yuan, S. Q.; Zheng, H. L.; Ebnet, K.; Yan, W.; Knoblich, J. A.; Gerlich, D. W. *EMBO J.* **2016**, *35*, 2386−2398.

(5) Chang, J.; Davis-Dusenbery, B. N.; Kashima, R.; Jiang, X.; Marathe, N.; Sessa, R.; Louie, J.; Gu, W.; Lagna, G.; Hata, A. *EMBO J.* **2013**, *32*, 3192−3205.

(6) Li, Y. S.; Wen, S. H.; Yao, X.; Liu, W. F.; Shen, J. T.; Deng, W. T.; Tang, J.; Li, C.; Liu, K. X. *Cell Death Dis.* **2017**, *8*, e3127.

(7) Zhao, C.; Sun, G. Q.; Li, S. X.; Lang, M. F.; Yang, S.; Li, W. D.; Shi, Y. H. *Proc. Natl. Acad. Sci. U. S. A.* **2010**, *107*, 1876−1881.

(8) Pencheva, N.; Tran, H.; Buss, C.; Huh, D.; Drobnjak, M.; Busam, K.; Tavazoie, S. F. *Cell* **2012**, *151*, 1068−1082.

(9) Laterza, O. F.; Lim, L.; Garrett-Engele, P. W.; Vlasakova, K.; Muniappa, N.; Tanaka, W. K.; Johnson, J. M.; Sina, J. F.; Fare, T. L.; Sistare, F. D.; Glaab, W. E. *Clin. Chem.* **2009**, *55*, 1977−1983.

(10) Kakkassery, V.; Schroers, R.; Coupland, S. E.; Wunderlich, M. I.; Schargus, M.; Heinz, C.; Wasmuth, S.; Heiligenhaus, A.; Ahle, G.; Lenoble, P.; Schlegel, U.; Schmiegel, W.; Dick, H. B.; Baraniskin, A. *Blood* **2017**, *129*, 3130−3133.

(11) Boeri, M.; Verri, C.; Conte, D.; Roz, L.; Modena, P.; Facchinetti, F.; Calabro, E.; Croce, C. M.; Pastorino, U.; Sozzi, G. *Proc. Natl. Acad. Sci. U. S. A.* **2011**, *108*, 3713−3718.

(12) Wu, H.; Ng, R.; Chen, X.; Steer, C. J.; Song, G. S. *Gut* **2016**, *65*, 1850−1860.

(13) Persson, H.; Sokilde, R.; Hakkinen, J.; Pirona, A. C.; Vallon-Christersson, J.; Kvist, A.; Mertens, F.; Borg, A.; Mitelman, F.; Hoglund, M.; Rovira, C. *Nat. Commun.* **2017**, *8*, 788.

(14) Yang, C. H.; Pfeffer, S. R.; Sims, M.; Yue, J. M.; Wang, Y. N.; Linga, V. G.; Paulus, E.; Davidoff, A. M.; Pfeffer, L. M. *J. Biol. Chem.* **2015**, *290*, 6037−6046.

(15) Belter, A.; Rolle, K.; Piwecka, M.; Fedoruk-Wyszomirska, A.; Naskret-Barciszewska, M. Z.; Barciszewski, J. *Sci. Rep.* **2016**, *6*, 24516.

(16) Siegel, R. L.; Miller, K. D.; Jemal, A. *Ca-Cancer J. Clin.* **2016**, *66*, 7−30.

(17) Weiss, F. U.; Marques, I. J.; Woltering, J. M.; Vlecken, D. H.; Aghdassi, A.; Partecke, L. I.; Heidecke, C. D.; Lerch, M. M.; Bagowski, C. P. *Gastroenterology* **2009**, *137*, 2136−2145.

(18) Yuen, T.; Wurmbach, E.; Pfeffer, R. L.; Ebersole, B. J.; Sealfon, S. C. *Nucleic Acids Res.* **2002**, *30*, e48.

(19) Rosenfeld, N.; Aharonov, R.; Meiri, E.; Rosenwald, S.; Spector, Y.; Zepeniuk, M.; Benjamin, H.; Shabes, N.; Tabak, S.; Levy, A.; Lebanony, D.; Goren, Y.; Silberschein, E.; Targan, N.; Ben-Ari, A.; Gilad, S.; Sion-Vardy, N.; Tobar, A.; Feinmesser, M.; Kharenko, O.; Nativ, O.; Nass, D.; Perelman, M.; Yosepovich, A.; Shalmon, B.; Polak-Charcon, S.; Fridman, E.; Avniel, A.; Bentwich, I.; Bentwich, Z.; Cohen, D.; Chajut, A.; Barshack, I. *Nat. Biotechnol.* **2008**, *26*, 462−469.

(20) Hildebrandt, N.; Spillmann, C. M.; Algar, W. R.; Pons, T.; Stewart, M. H.; Oh, E.; Susumu, K.; Diaz, S. A.; Delehanty, J. B.; Medintz, I. L. *Chem. Rev.* **2017**, *117*, 536−711.

(21) Han, L.; Liu, P.; Zhang, H. J.; Li, F.; Liu, A. H. *Chem. Commun.* **2017**, *53*, 5216−5219.

(22) Zhu, L. P.; Lu, H.; Hao, D.; Wang, L. L.; Wu, Z. H.; Wang, L. J.; Li, P.; Ye, J. H. *ACS Appl. Mater. Interfaces* **2017**, *9*, 38537−38544.

(23) Yang, D. W.; Tang, Y. G.; Miao, P. *TrAC, Trends Anal. Chem.* **2017**, *94*, 1−13.

(24) Ge, L.; Sun, X. M.; Hong, Q.; Li, F. *ACS Appl. Mater. Interfaces* **2017**, *9*, 32089−32096.

(25) Li, Y.; Pu, Q. L.; Li, J. L.; Zhou, L. L.; Tao, Y. Y.; Li, Y. X.; Yu, W.; Xie, G. M. *Microchim. Acta* **2017**, *184*, 4323−4330.

(26) Liu, X. J.; Song, M. M.; Hou, T.; Li, F. *ACS Sens.* **2017**, *2*, 562−568.

(27) Ou, S.; Xu, T.; Liu, X.; Yu, X. Y.; Li, R.; Deng, J.; Yuan, J. X.; Chen, Y. M. *Sens. Actuators, B* **2018**, *255*, 3057−3063.

(28) Wang, L.; Su, D.; Berry, S. N.; Lee, J.; Chang, Y. T. *Chem. Commun.* **2017**, *53*, 12465−12468.

(29) Miao, P.; Tang, Y. G.; Mao, Z. Q.; Liu, Y. Z. *Part. Part. Syst. Charact.* **2017**, *34*, 1600405.

(30) Miao, P.; Ning, L. M.; Li, X. X. *Anal. Chem.* **2013**, *85*, 7966−7970.

(31) Hou, T.; Li, W.; Liu, X. J.; Li, F. *Anal. Chem.* **2015**, *87*, 11368−11374.

(32) Zhu, D.; Liu, W.; Zhao, D. X.; Hao, Q.; Li, J.; Huang, J. X.; Shi, J. Y.; Chao, J.; Su, S.; Wang, L. H. *ACS Appl. Mater. Interfaces* **2017**, *9*, 35597−35603.

(33) Su, S.; Cao, W. F.; Liu, W.; Lu, Z. W.; Zhu, D.; Chao, J.; Weng, L. X.; Wang, L. H.; Fan, C. H.; Wang, L. H. *Biosens. Bioelectron.* **2017**, *94*, 552−559.

(34) Miao, P.; Wang, B. D.; Chen, X. F.; Li, X. X.; Tang, Y. G. *ACS Appl. Mater. Interfaces* **2015**, *7*, 6238−6243.

(35) Su, S.; Wu, Y.; Zhu, D.; Chao, J.; Liu, X. F.; Wan, Y.; Su, Y.; Zuo, X. L.; Fan, C. H.; Wang, L. H. *Small* **2016**, *12*, 3794−3801.

(36) Wang, T. Y.; Viennois, E.; Merlin, D.; Wang, G. L. *Anal. Chem.* **2015**, *87*, 8173−8180.

(37) Miao, P.; Tang, Y. G.; Wang, B. D.; Jiang, C. M.; Gao, L. Q.; Bo, B.; Wang, J. *Electrochim. Acta* **2016**, *190*, 396−401.

(38) Gai, P. P.; Gu, C. C.; Li, H. Y.; Sun, X. Z.; Li, F. *Anal. Chem.* **2017**, *89*, 12293−12298.

(39) Ge, Z. L.; Lin, M. H.; Wang, P.; Pei, H.; Yan, J.; Shi, J. Y.; Huang, Q.; He, D. N.; Fan, C. H.; Zuo, X. L. *Anal. Chem.* **2014**, *86*, 2124−2130.

(40) Zhang, X.; Wu, D. Z.; Liu, Z. J.; Cai, S. X.; Zhao, Y. P.; Chen, M.; Xia, Y. K.; Li, C. Y.; Zhang, J.; Chen, J. H. *Chem. Commun.* **2014**, *50*, 12375−12377.

DOI: 10.1021/acs.analchem.7b05447
Anal. Chem. 2018, 90, 2395−2400